Research Article

Ahmed Abdrabou*, Medhat Abdallah, Gilan M. Sultan, Mohamed Mostafa, Hind Bayoumi, Ramy Magdy, Mohamed A. Abd El Kader, Nagmeldeen M. Hamza, Dina Mamdouh, Hassan M. Elsayed, Eltayeb Abbas, Hussein M. Kamal

Tutankhamun's Polychrome Wooden Shawabtis: Preliminary Investigation for Pigments and Gilding Characterization and Indirect Dating of Previous Restorations by the Combined Use of Imaging and Spectroscopic Techniques

https://doi.org/10.1515/opar-2022-0223
received April 26, 2021; accepted February 21, 2022

Abstract: To the best of our knowledge, such a detailed study on polychrome wooden shawabtis of King Tutankhamun (18th Dynasty in ancient Egypt) has not been reported in the literature, so the purpose of our study is to noninvasively identify the polychrome layers and previously applied materials for a number of wooden shawabtis that belong to King Tutankhamun through a protocol based on imaging techniques integrated with single-spot spectroscopic techniques. In the first step, imaging techniques (visible, ultraviolet induced visible luminescence, ultraviolet reflected, visible-induced infrared luminescence, infrared reflected, and infrared false color) and optical microscopy were applied to gather information and provide evidence on the distribution of original and previously applied materials on the polychrome surfaces. In the second step of our work, we analyzed the selected areas with single-spot analyses (handheld X-ray fluorescence spectroscopy and visible reflectance spectroscopy) and X-ray diffraction analysis. The materials of the previous restoration interventions were studied by Fourier transform infrared spectroscopy. The application of a protocol based on imaging techniques integrated with data obtained from single-spot spectroscopic techniques allowed the characterization of a remarkable number of polychrome layers and some previous restoration materials and mapping of their distribution on the original surface, which provides not only essential data for the follow-up treatment and conservation works but also offers important information for the study of polychrome wooden shawabtis of other periods in ancient Egypt.

Keywords: shawabtis, Tutankhamun, multispectral imaging, orpiment, handheld XRF

*** Corresponding author: Ahmed Abdrabou,** Wood Conservation Laboratory, Grand Egyptian Museum – Conservation Center (GEM.CC), Giza, Egypt, e-mail: ahmed_abdrabou87@yahoo.com
Medhat Abdallah: Directorate of Conservation, Saqqara Store Rooms, Giza, Egypt
Gilan M. Sultan, Mohamed Mostafa, Hind Bayoumi, Ramy Magdy, Mohamed A. Abd El Kader: Wood Conservation Laboratory, Grand Egyptian Museum – Conservation Center, Giza, Egypt
Nagmeldeen M. Hamza: Organic Conservation Laboratory, Grand Egyptian Museum-Conservation Center, Giza, Egypt
Dina Mamdouh: FTIR Laboratory, Grand Egyptian Museum-Conservation Center, Giza, Egypt
Hassan M. Elsayed: Department of Tutankhamun Collection, Grand Egyptian Museum, Giza, Egypt
Eltayeb Abbas: Directorate of Archaeological Affairs, Grand Egyptian Museum, Giza, Egypt
Hussein M. Kamal: Directorate of Conservation Affairs, Grand Egyptian Museum-Conservation Center, Giza, Egypt
ORCID: Ahmed Abdrabou 0000-0003-3423-3884

1 Introduction

Shawabtis (also called shabtis or ushabtis) are funerary statuettes found in ancient Egyptian burial assemblages that have been traditionally interpreted as workers enlisted by their owners to conduct work on their behalf in the afterlife. They became popular in the Middle Kingdom (2055–1650 BCE) and were abundantly produced until they decreased in usage toward the end of the Ptolemaic Period (332–30 BC) (Hoving, 1978; Schneider, 1977).

Shawabtis found in King Tutankhamun's tomb come in a variety of styles and materials. The tomb contains 413 shawabtis of which 365 are workmen, 36 are overseers, and 12 are directors. These shawabtis were housed in 24 boxes, 10 of which were recovered from the northeast corner of the treasury and 14 from the annex. They were also made of a variety of materials, including 189 shawabtis of wood, 121 of faience, 42 of alabaster, 8 of limestone, 3 of black granite, and 50 of quartzite (Carter, 1933; Reeves, 1990).

The multidisciplinary analytical techniques of polychrome artifacts, belonging to museum collections, particularly unique objects, which emphasize the necessity of working with noninvasive techniques, have gained much interest in recent years and have been reported by many authors to study the original polychrome layers as well as modern restoration interventions in order to yield more information useful for conservation processes (Abdallah, Abdrabou, & Kamal, 2020; Abdrabou, Abdallah, Shaheen, & Kamal, 2018; Abdrabou, El Hadidi, Hamed, & Abdallah, 2018; Abdrabou, Abdallah, Nabil, Matsuda, & Kamal, 2019; Bonizzoni et al., 2018; Bracci et al., 2015; Brunel-Duverger, Laval, Lemasson, Brodie-Linder, & Pagès-Camagna, 2019; Dyer & Sotiropoulou, 2017; Gard et al., 2020; Ismail, Abdrabou, & Abdallah, 2016).

Like most of the objects in the tomb of Tutankhamun, some shawabtis were treated by Lucas before being transferred to the Egyptian Museum, where they were displayed. In 2017, 105 wooden shawabtis were transported to the Grand Egyptian Museum's Conservation Center for investigation and conservation works in preparation for the exhibition at the new museum. Twelve shawabtis were the subject of the first targeted diagnostic study inside the Wood Conservation Laboratory at the Grand Egyptian Museum's Conservation Center (GEM CC). So, the primary objective of our current study is to identify the chemical composition of the pictorial layers used to decorate the shawabtis as well as to present a panoramic view of the previous restoration materials and their distribution on the original surface via a wide array of noninvasive analytical techniques, which provides not only essential data for the study of polychrome wooden shawabtis of King Tutankhamun with those from different periods in ancient Egypt, but also important information for the follow-up treatment and conservation works. The selected analytical protocol aimed to limit the sampling as much as possible, while at the same time obtaining a large set of significant data. The analytical investigations that have been designed for this type of object represent the first step in the characterization of polychrome wooden shawabtis that belong to King Tutankhamun.

2 Materials and Methods

2.1 The Studied Artifacts

In this work were investigated, by means of imaging and spectroscopic techniques, 12 polychrome wooden shawabtis from the collection of King Tutankhamun (Figure 1). The numbers, locations inside the tomb, dimensions, and descriptions of these shawabtis are summarized in Table 1.

2.2 Methodology

In our work, the sequence of investigation and analysis began with multispectral imaging followed by closer inspection under a microscope to characterize the spatial distribution of pigments and later applied materials.

Figure 1: The selected shawabtis from King Tutankhamun collection as numbered in Table 1, and the spots marking the locations listed in Table 3 from where analysis by single-spot spectroscopic techniques were performed (indicated by English numbers); a) Shawabti GEM GEM 3163; b) Shawabti GEM 3414; c) Shawabti GEM 3429; d) Shawabti GEM 3173; e) Shawabti GEM 3511; f) Shawabti GEM 3503; g) Shawabti GEM 3528; h) Shawabti GEM 3499; i) Shawabti GEM 3491; j) Shawabti GEM 3651; k) Shawabti GEM 3467; l) Shawabti GEM 3452.

Based on the data from the technical imaging and detailed examination, spots of each area of interest were then analyzed using hand held X-ray fluorescence (XRF) and Vis-RS. After this, the measurements by X-ray diffraction (XRD) were directly performed on the same spots (made by XRF) in a nondestructive mode without any sample preparation. Finally, four samples from the previous restoration materials were carefully scraped off with a metallic scalpel for analysis by Fourier transform infrared spectroscopy (FTIR).

2.2.1 Multispectral Imaging (MSI)

Technical images were captured with a Nikon D90 DSLR (CMOS sensor) digital camera that had been modified for "full spectrum (c. 350–1,000 nm)" by removing the inbuilt UV-infrared reflected (IR) blocking filter and fitted with a Tokina Macro 35 mm F/2.8D DX lens that was used at its widest F-stop setting (2.8) to capture all luminescence images with shutter speeds ranging from 0.8 to 8 s. The camera was operated fully

Table 1: A summary of the shawabtis showing the numbers, dimensions, location inside the tomb, and description

Image no.	Object no.	Length (cm)	Location in the tomb	Carter description [The Griffith institute (2000–2004)]
a	Carter No: 611a JE 60914 GEM 3163	23.5	with group of shawabtis inside a kiosk (Carter no. 611)	Made of wood wearing wig striated with blue, beard, eyes, and eyebrows black, eyeballs white, holding in hands the pick, hoe, and two baskets, and the inscription incised and filled in with blue
b	Carter No: 323j JE 60864 GEM 3414	25.5	With a group of shawabtis inside a kiosk (Carter no. 323) Center of chamber	Made of wood covered with red painted layers, details of face and beard black; text blue, holding the hoe in R. hand, pick in L. hand, and a basket in both hands
c	Carter No: 319c JE 60895 GEM 3429	27	With a group of shawabtis inside a kiosk (Carter no. 319)	Made of wood covered with red painted layers, details of face and beard black, text blue, and holding an ankh sign in both hands. Treated with dilute celluloid solution
d	Carter No: 324a JE 60918 GEM 3173	23	With group of shawabtis inside a kiosk (Carter no. 324)	Made of wood smeared with yellow; wearing wig striated with blue, while beard, eyes, and eyebrows black, eyeballs white, and holding a pick, hoe, and two baskets in hands. The inscription incised and filled in with blue. Treated with dilute celluloid solution
e	Carter No: 323n JE 60851 GEM 3511	24.5	With a group of shawabtis inside a kiosk (Carter no. 323) Center of chamber	Made of wood and covered with red painted layers in the shape of a mummy; wearing a round wig painted with blue, beard and eyebrows with black, and eyeballs and collarettes with white
f	Carter No: 418e JE 60848 GEM 3503	22.5	With a group of shawabtis inside a kiosk (Carter no. 418) Center of chamber	Made of wood and covered with red painted layers in the shape of a mummy; wearing a round wig painted with dark blue, beard and eyebrows with black, and eyeballs and collarettes with white
g	Carter No: 323b JE 60856 GEM 3528	27.3	With a group of shawabtis inside a kiosk (Carter no. 323)	Made of wood and covered with gesso painted layers (red–yellow–black), holding a pick in the left hand and a basket in both hands. Treated with dilute celluloid solution
h	Carter No: 602b JE 60846 GEM 3499	29.5	With a group of shawabtis inside a kiosk (Carter no. 602b) Center of chamber	Made of wood and covered with painted light red layers, wearing a painted black round wig with gilded uraeus, gilded temple band, and bead collarette round the neck, holding a gilded band of linen in the left hand and a gilded flagellum, and round the wrists gilded bracelets in the right hand. Eyes and eyebrows black and eyeballs white
i	Carter No: 602d JE 60844 GEM 3491	26.4	With a group of shawabtis inside a kiosk (Carter no. 602)	Made of wood and covered with painted light red layers, wearing h3t head-dress with gilded uraeus, gilded temple band, and bead collarette round the neck, holding a gilded band of linen in the left hand and a gilded flagellum, and round the wrists gilded bracelets in the right hand. Eyes and eyebrows black and eyeballs white
j	Carter No: 512a JE 60783 GEM 3651	23.6	With a group of shawabtis inside a kiosk (Carter no. 512)	Made of wood and covered with gilded gesso layers, wearing a head-dress and beard; holding a pick and a hoe in hands. The eyes and eyebrows painted black

(*Continued*)

Table 1: *Continued*

Image no.	Object no.	Length (cm)	Location in the tomb	Carter description [The Griffith institute (2000–2004)]
k	Carter No: 608d JE 60813 GEM 3467	24.2	With a group of shawabtis inside a kiosk (Carter no. 608)	Made of wood and covered with gilded gesso layers wearing a round wig and beard. The eyes and eyebrows painted black. Text and wig filled with blue
l	Carter No: 512c JE 60807 GEM 3452	23.4	With a group of shawabtis inside a kiosk (Carter no. 512)	Made of wood and covered with gilded gesso layers, wearing a round wig and beard; the eyes and eyebrows painted black

manually and tethered to a computer to allow sharp focusing in nonvisible modes (IR and UV) using live view mode with the picture style set to "Neutral" and an ISO speed of 100. Except for the acquisition of UV-induced visible luminescence images, where it was set to a color temperature of 6,500 K, white balance was set to "Custom." To calibrate the camera, an X-Rite ColorChecker Passport and a reference gray scale were used (Abdrabou, Hussein, Sultan, & Kamal, 2022; Cosentino, 2015; Dyer, Verri, & Cupitt, 2013).

In each case, the shawabti was illuminated by two radiation sources that were symmetrically positioned at approximately 45° with respect to the camera's focal axis and at approximately the same height. To select the wavelength range of interest, a filter or combination of filters was placed in front of the camera lens. Table 2 summarizes the filters and radiation sources used for imaging techniques. All images were captured as RAW files and converted to TIF (tagged image file) format and a set of recommended presets which turn-off all enhancements (e.g., recovery, fill light, blacks, contrast, brightness, clarity, saturation, as well as setting the tone-curve to linear) were applied using Adobe Photoshop. Post-processing procedures for the calibration of the visible (VIS), ultraviolet induced visible luminescence (UVL), ultraviolet reflected (UVR), visible-induced luminescence (VIL), and IR images as well as the creation of infrared false color (IRFC) images are then carried out using the "British Museum (BM) workspace" and nip2 software (Martinez & Cupitt, 2005) as described by Dyer et al. (2013).

2.2.2 Optical Microscopy (OM)

For detailed observations of the polychrome layers, we used a Zeiss Stereo DV 20 (portable stereomicroscope) equipped with an Axio Cam MRC5 with an optical zoom of 28 up to 560×.

2.2.3 XRF

The painted preparation layers were nondestructively analyzed by a handheld XRF (HH-XRF) spectrophotometer using a Thermo Scientific Niton XL3t with a "GOLDD" detector. It was placed in contact with the selected area, and the X-ray spot size was 3 mm in diameter. The X-ray tube has a Ag anode of 50 kV and 200 μA. The standardization modes selected are the "Cu/Zn Mining", which includes the elements of interest for the analysis of painted preparation layers (e.g., Ca, S, Si, Cu, Fe, As, Pb, Sn, Cl, and P) and the "precious metal" mode, which includes the elements of interest for the analysis of gilding (e.g., Au, Ag, and Cu). This analysis uses four separate filters to determine the concentrations in percentage of elements: a high filter (30 s counting time), a main filter (30 s), a low filter (30 s), and a light filter (30 s), leading to a total measurement time of 120 s per analysis. The software utilizes the Fundamental Parameters algorithm to determine the concentrations of each element. The spectra obtained from the XL3t were downloaded to a computer for analysis by the Thermo Scientific NDT program. The total points considered for HH-XRF analyses were chosen for different colors and conservation situations following suggestions from the results of imaging analyses.

Table 2: A summary of the filters and radiation sources used for imaging techniques

Imaging techniques	Filters	Radiation sources
VIS	X-Nite CCI	White fluorescent lamps
UVL	UV/IR Baader filter + X-Nite CCI	Ultraviolet LED lamps (365 nm)
UVR	A Schneider B + W 403 + X-NiteCC1	Ultraviolet LED lamps (365 nm)
VIL	A Schott RG840 cut-on filter	White LED lamps
IR	A Schott RG840 cut-on filter	Infrared LED lamps (900 nm)
IRFC	Made by digitally editing the VIS and IR images in Adobe Photoshop	

2.2.4 Vis-RS

A Konica Minolta Spectrophotometer CM-2600d was used to record the reflectance spectra of the painted layers under standard illuminant d65 (the di:8°/de:8° geometry (diffused illumination, 8° viewing angle), including the specular component (measuring area: circular area with a diameter of 5 mm). Spectra are collected along a 400–700 nm wavelength range every 10 nm. The light diffused in the integrating sphere is received by the illumination-monitoring optical system and guided to a sensor. The light reflected from the painted surfaces and the diffused light are divided into each wavelength component by a measuring optical system and illumination-monitoring optical sensor, respectively, and the signals proportional to the light intensity of each component are output to the analog processing circuit.

2.2.5 XRD

PANalytical pro model PW3040 XRD with a Cu anode at 30 mA/40 kV was directly performed on the shawabtis. Each shawabti was placed inside an XRD apparatus on a sample holder, and an approximately flat surface of each color was exposed to the X-ray beam. Diffraction patterns were interpreted using X'Pert HighScore software.

2.2.6 FTIR

FTIR measurements were conducted using an FTIR spectrometer (IRPrestige-21, Shimadzu) in the 400–4,000 cm^{-1} range, with a resolution of 8 cm^{-1}. Samples of the previous restoration materials were identified by comparing the obtained spectra with literature data (Derrik, Stulik, & Landy, 1999) and standards created in the FTIR laboratory at the GEM CC.

3 Results and Discussion

3.1 Analysis of Polychrome Layers

The chromatic palette of these shawabtis includes blue, yellow, red, white, black, and gilding. Table 3 summarizes imaging, OM, HH-XRF, and XRD analysis results for the different polychrome layers of these shawabtis.

3.1.1 Blue and Greenish Hue Painted Layers

In the VIL images (Figures 2b and 3b), the blue and greenish blue painted layers appeared as bright white, while all other materials appeared dark. The luminescence of such areas indicates the presence of Egyptian blue (Accorsi et al., 2009; Amenta, 2014; Abdallah & Abdrabou 2018). According to XRF spectra of the blue painted layer (Figure 2c), the elements that presented the highest concentrations were silicon (Si), copper (Cu), calcium (Ca), and sulfur (S). This result provides strong evidence for the presence of Egyptian blue pigments, confirming the corresponding visible reflectance spectrum (Figure 2d), which matched published spectra of Egyptian blue with an inflection point at about 630 nm (Abdrabou, et al., 2022; Aceto et al., 2014; Edreira, Feliu, Fernández-Lorenzo, & Martín, 2001). The presence of S in the blue regions would suggest the presence of gypsum, whereas the presence of tin (Sn) impurities in the XRF analysis (Table 1) allowed us to assume that a bronze scrap was used to produce the Egyptian blue pigment (Abdrabou et al., 2018; Jaksch,

Table 3: A summary of imaging, OM, HH-XRF, and XRD analysis results for the painted layers

Object no.	Spot no.	Color	Imaging				OM	Elements detected by XRF	XRD results
			UVR	UVL	IR	VIL			
GEM 3163JE 60914	1	Blue	Dark	None	Dark	Bright white	Blue particles	**Cu, Ca, Si**, Fe, S, Sn, K, Cl, Ti, Sr, As	Cuprorivaite-Gypsum
	2	Black	Dark	None	Black	None	Fine black particles	**Ca**, Fe, S, Si, Cl, K, As, Ti	—
GEM 3414JE 60864	3	Blue	Dark	None	Dark	Bright white	Blue particles	**Cu, Ca, Si, Fe, As, S**, Al, K, Ti, Cl, Sn,	Cuprorivaite-Gypsum
	4	Red	Dark	None	Bright	None	Red particles with some single yellow particles	**Fe, As, Ca, S, Si**, Al, Cl, K, Ti	Hematite-Quartz
	5	Black	Dark	None	Black	None	Fine black particles	**Fe, Ca, As, S, Si**, Al, Cl, K, Ti	—
GEM 3429JE 60895	6	Greenish Blue	Dark	None	Dark	Bright white	Blue crystalline matrix with green tone	**Cu, Ca, Si**, Fe, S, As, Sn, Cl, K, Sr	—
	7	Red	Dark	None	Bright	None	Red particles with some single yellow particles	**Ca, Fe, As, S, Si**, Al, Cl, K, Ti	Hematite-Quartz
	8	Black	Dark	None	Black	None	Fine black particles	**Ca, Fe, As, S, Si**, Al, Cl, K, Ti	—
GEM 3173JE 60918	9	Greenish Blue	Dark	None	Dark	Bright white	Blue crystalline matrix with green tone	**Cu, Ca, Si**, Fe, Cl, Sn, S, As, K, Sr,	Cuprorivaite-Calcite-Quartz
	10	Yellow	Dark	Yellow	Bright	None	yellow particles	**As, Ca, Fe, S, Si**, K, Ti, Sr	—
	11	Black	Dark	None	Black	None	Fine black particles	**Ca, Fe**, S, Si, Cl, K, P, As, Ti	—
GEM 3511JE 60851	12	Blue	Dark	None	Dark	Bright white	Blue particles	**Cu, Ca, Si**, Fe, S, As, Sn, Cl, K, Sr,	Cuprorivaite-Gypsum
	13	Dark blue	Dark	None	Dark	Bright white	Dark blue particles	**Cu, Ca, Si**, Fe, S, As, Sn, Cl, K, Sr,	—
	14	Red	Dark	None	Bright	None	Red particles with some single yellow particles	**Fe, Ca, As, Si, S**, Al, Cl, K, Ti	Hematite-Quartz
	15	White	Bright	White	Bright	None	White particles with single yellow and blue particles	**Ca, As, Fe, Si, S**, Al, Cl, K, Ti, Cu	Gypsum-Weddellite-Quartz
	16	Black	Dark	None	Black	None	Fine black particles with some single yellow particles	**Fe, Ca, As, S**, Si, Al, Cl, K, Ti, Cu	—
GEM 3503JE 60848	17	Greenish blue	Dark	None	Dark	Bright white	Blue crystalline matrix with a green tone	**Cu, Ca, Si**, Fe, S, As, Sn, Cl, K, Sr,	Cuprorivaite-Calcite-Quartz

(*Continued*)

Table 3: *Continued*

Object no.	Spot no.	Color	Imaging				OM	Elements detected by XRF	XRD results
			UVR	UVL	IR	VIL			
	18	Red	Dark	None	Bright	None	Red particles with some single yellow particles	**Fe, Ca, As, Si, S**, Al, Cl, K, Ti	Hematite-Quartz
	19	White	Bright	White	Bright	None	White particles with some single yellow and blue particles	**Ca, As, Fe, Si, S**, Al, Cl, K, Ti, Cu	Gypsum-Weddellite-Quartz
	20	Black	Dark	None	Black	None	Fine black particles with some single yellow particles	**Fe, Ca, As, Si, S**, Al, Cl, K, Ti	—
GEM 3528JE 60856	21	Yellow	Dark	Yellow	Bright	Some particles appeared as white bright	Yellow particles with some blue particles	**Ca, As, Fe, S, Si, Cu**, K, Ti, Sr	—
	22	Red	Dark	None	Bright	None	Red particles	**Ca, Fe**, Si, S, Cl, K, Ti, As	Hematite-Calcite
	23	Black	Dark	None	Black	None	Fine black particles	**Ca, Fe**, Si, S, Cl, K, Ti, As, Sr	—
GEM 3499JE60846	24	Red	Dark	None	Bright	None	Red particles with some single yellow particles	**Fe, Ca, As, S, Si**, Al, K, Ti	Hematite-Quartz
	25	Black	Dark	None	Black	None	Black particles	**Ca, Fe, S, Si, As**, P, K, Ti	
	26	Yellow gilding	—	None	—	—		Au, Ag, Cu	—
	27	Dark gilding	—	None	—	—		Au, Ag, Cu	—
JE60844	28	Red	Dark	None	Bright	None	Red particles with some single yellow particles	**Fe, Ca, As, S, Si**, Al, K, Ti	Hematite-Quartz
	29	Yellow gilding	—	None	—	—		**Au, Ag, Cu**	—
	30	Dark gilding	—	None	—	—		**Au, Ag, Cu**	—
GEM 3651JE 60783	31	Yellow gilding	—	None	—	—		Au, Ag, Cu	—
	32	Dark gilding	—	None	—	—		Au, Ag, Cu	—
	33	Dark gilding	—	None	—	—		Au, Ag, Cu	
	34	Yellow previous material	Dark	Very dark	—	—		**Fe**, S, Zn, Ba, Ca, Sr	—
GEM 3467JE60813	35	Blue	Dark	None	Dark	Bright white	Blue particles	**Cu, Ca, Au, Si**, Fe, Ti, Sn, Ag, Cl, As	—
	36	Yellow gilding	—	Green	—	—		Au, Ag, Cu	—
GEM 3452JE 60807	37	Yellow gilding	—	Yellow	—	—		Au, Ag, Cu	—
	38	Yellow gilding	—	Green	—	—		Au, Ag, Cu	—

Note: Elements in boldface are correlated to the main pigment mineral.

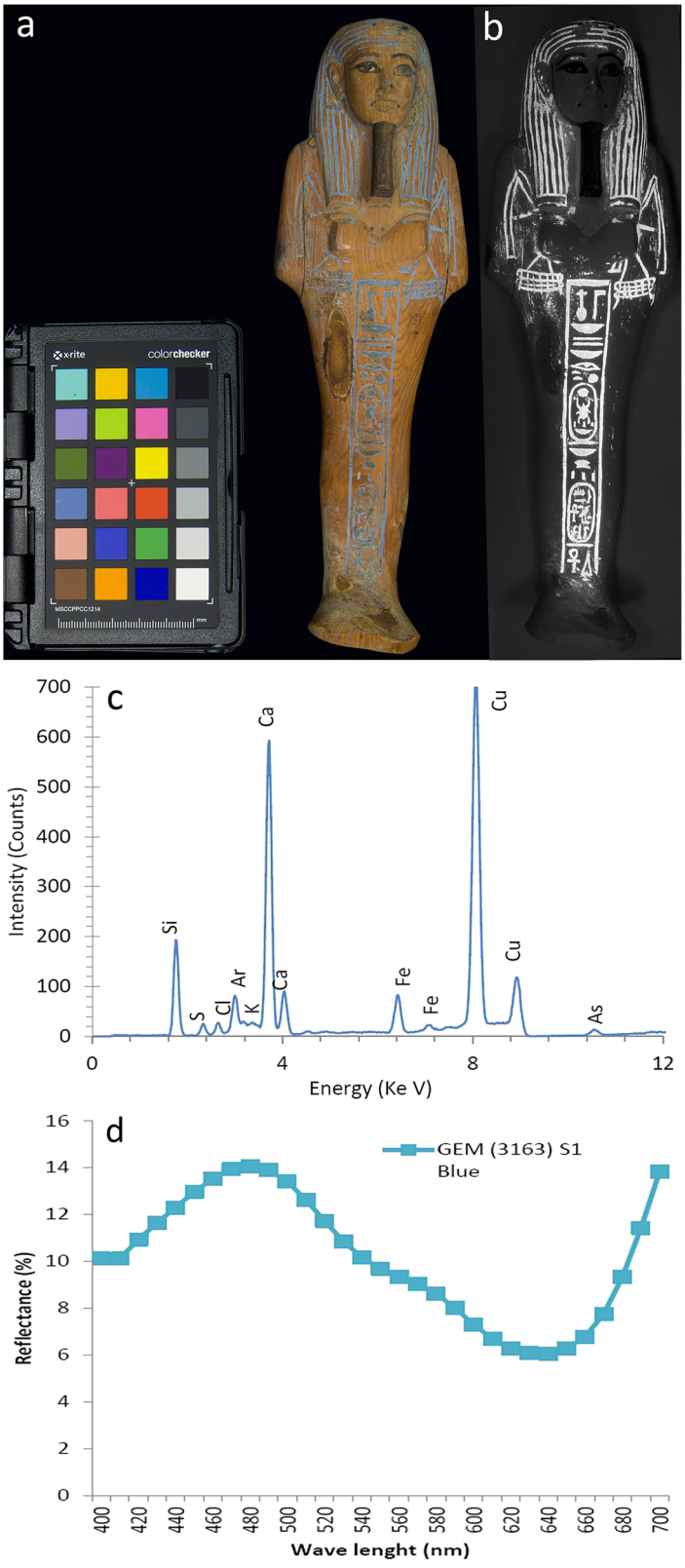

Figure 2: Characterization of the blue painted layer (Object GEM 3163, Spot 1): (a) visible image; (b) VIL image; (c) XRF spectrum; and (d) visible reflectance spectrum.

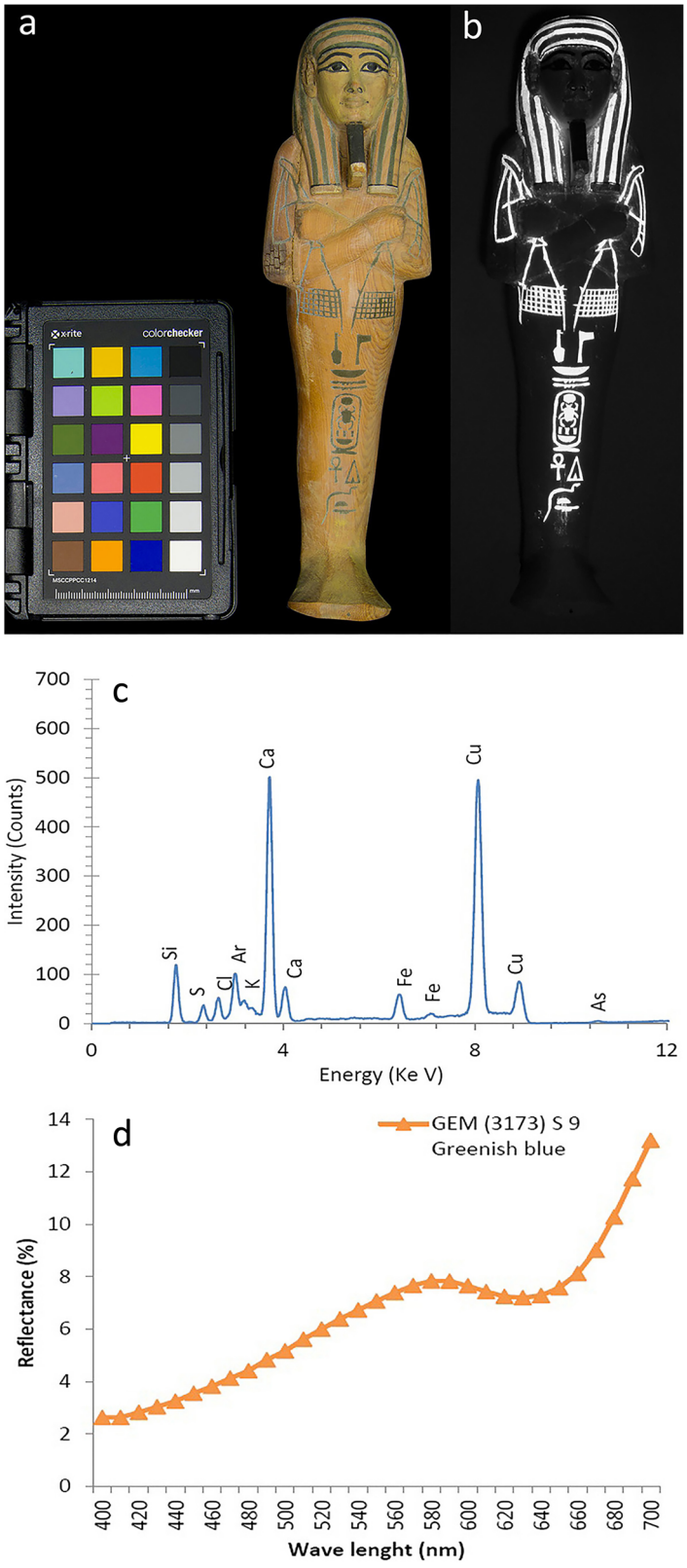

Figure 3: Characterization of the greenish blue painted layer (Object GEM 3173, Spot 9): (a) visible image; (a) VIL image; (c) XRF spectrum; and (d) visible reflectance spectrum.

Seipel, Weiner, & El Goresy, 1983). Applying XRD (Figure 4a) confirmed the presence of gypsum and cuprorivaite (the main component of Egyptian blue) for the blue painted layers in accordance with the attribution made after the VIL and XRF spectra. The Egyptian blue pigment was the first synthetic pigment ever produced by man and dates to the Protodynastic period in Egypt (around 3200–3000 BC). It was found on a Protodynastic period bowl with markings attributed to the Scorpion King and was extensively used from the 4th Dynasty in Egypt until the end of the Roman period (Abdrabou, Abdallah, & Kamal, 2017; Corcoran, 2016; Ganio et al., 2015; Mirti et al., 1995). Egyptian blue is a multicomponent pigment made from locally derived component minerals of copper, calcium, silica (in the form of quartz, SiO_2), and about 1% flux, usually comprising lime (CaO) from calcium carbonate to form calcium copper tetrasilicate crystals (cuprorivaite: $CaCuSi_4O_{10}$), the chromophore in the Egyptian blue. This material can be characterized by its blue tabular crystals, which have been fritted in an oxidizing atmosphere at 850–1,100°C (Hatton, Shortland, & Tite, 2008; Ismail et al., 2016; Lee, 1997; Pradell, Salvado, Hatton, & Tite, 2006).

In general, Egyptian blue is a very stable pigment, and there are examples to be seen in Egypt that have been exposed for thousands of years without the loss of color, as seen in Figure 1. However, some objects painted with the Egyptian blue pigment show some discoloration that varies considerably, from a relatively greenish hue to black (Daniels, Stacey, & Middleton, 2004). In the studied shawabtis GEM no. 3429, 3173, and 3503, the microscopic investigation reveals that the greenish hue is a surface phenomenon, with what appears to be fresh, bright blue pigment lying beneath the greenish layer. Moreover, the microscopic investigation did not show any yellow particles in the greenish hue areas, so the hypothesis of a mixture

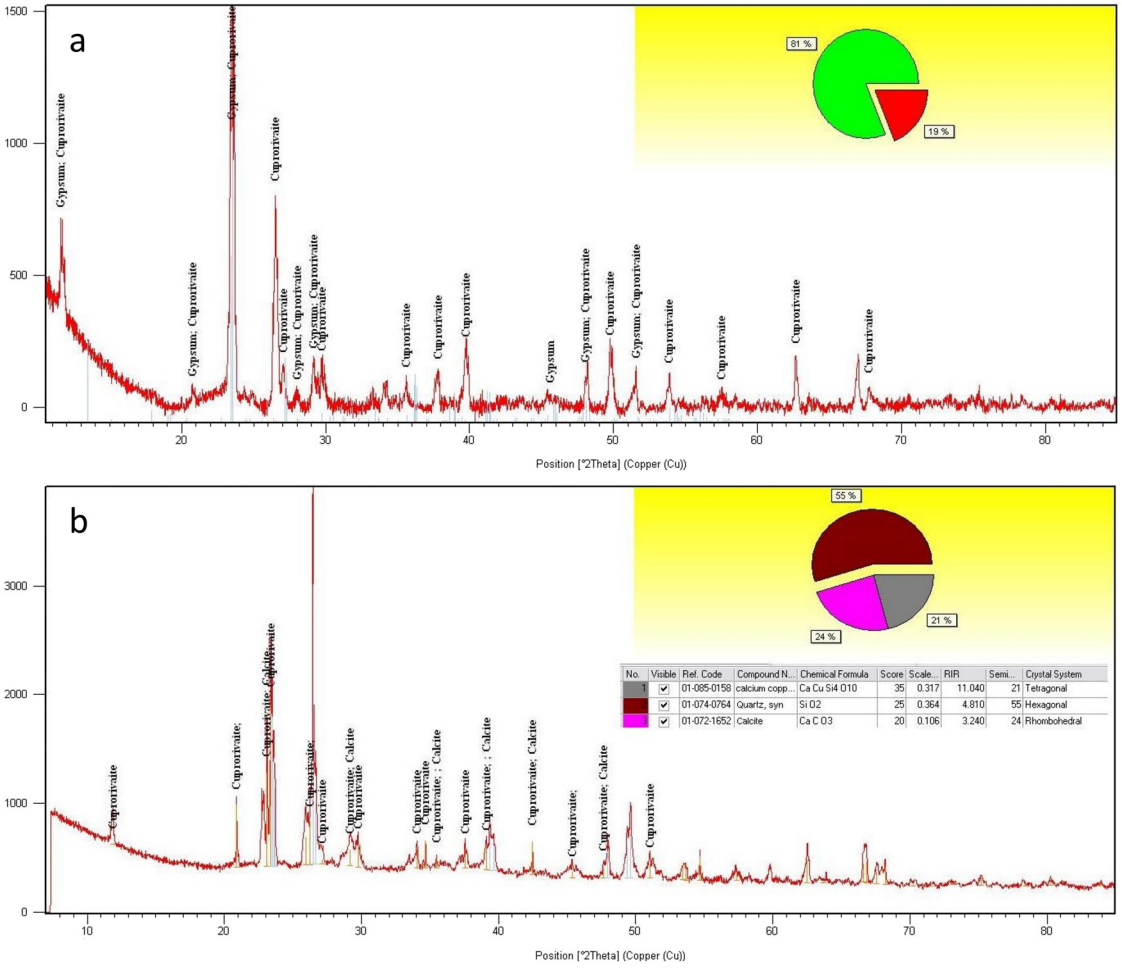

Figure 4: XRD patterns of: (a) the blue painted layer (Object GEM 3163, Spot 1) and (b) the greenish blue painted layer (Object GEM 3173, Spot 9).

of Egyptian blue and yellow pigments can be discarded. It is possible that the greenish hue is due to the degradation of the Egyptian blue pigment to atacamite or its polymorphs through the process known as "copper chloride cancer" (Abadir, 2014) or due to the darkening of organic materials used as binders or previous consolidation materials (Daniels et al., 2004). According to the XRF results of the greenish hue areas (Figure 3c), the elements that presented the highest intensities were Si, Cu, and Ca, with a significant amount of chlorine (Cl). This result provides strong evidence for the presence of the Egyptian blue pigment, confirming the corresponding visible reflectance spectrum (Figure 3d), which matched published spectra of Egyptian blue, with shifting in the reflectance ranging between 400 and 600 nm in the greenish blue painted layer due to its discoloration. The presence of Cl in the greenish hue areas would probably point to the presence of halite or a chlorine-containing solid phase and, considering the chemical reactivity of cuprorivaite, this solid phase could be atacamite, $Cu_2(OH)_3Cl$, or one of its polymorphs, paratacamite or clinoatacamite, which are products of the degradation of Egyptian blue when in contact with high-chloride concentration solutions. By applying XRD to the greenish hue areas (Figure 4b), apart from calcite and quartz, cuprorivaite (the main component of Egyptian blue) was detected. The absence of atacamite or its polymorphs in the diffractogram could be due to a lower percentage of atacamite or that the new phase formed on the surface of the blue pigment is amorphous. Consequently, the XRD technique is not able to detect it. Therefore, further analysis using Raman spectroscopy and gas chromatography/mass spectrometry will be necessary to determine its identity more precisely. This phenomenon (the coexistence of Egyptian blue and atacamite on blue-green colors) has already been reported by many authors (Giménez, 2015; Green, 2001; Lee, 1997; Riederer, 1977).

3.1.2 Yellow Painted Layer

The yellow fluorescence of yellow areas of shawabti no. 3528 under UV (Figure 5b) suggests that a yellow painted layer was probably made of arsenic (As)-based pigments such as orpiment since it had fluorescence properties (Abdrabou et al., 2018; Stuart, 2007). In addition, the microscopic examination revealed large yellow particles in a granular form, as well as the presence of some single particles of the blue pigment in the yellow painted layer (Figure 5d). These single particles appeared as bright white in the VIL image (Figure 5c), which refers to the Egyptian blue pigment. Moreover, comparing the VIS and VIL images (Figure 5a and c) allowed for the surviving Egyptian blue pigment to be mapped, and it is clear that its presence is much more extensive than what was discernible with the naked eye. In Figure 5e, the XRF spectrum of the yellow painted layer is shown. It shows a high intensity of As, Ca, Cu, S, Si, and Fe. It is interesting to note that Cu, Ca, and Si are detected in the yellow areas, clearly related to the single particles of Egyptian blue in accordance with the attribution obtained by VIL imaging. The presence of these blue single particles in the yellow paint layer could be accidental impurities due to the use of a dirty brush or could be added to achieve a higher intensity of the yellow sensation. The high intensity of As and S provides strong evidence for the presence of an arsenic sulfide pigment that is most likely orpiment (As_2S_3) in a nearly pure form, as confirmed by Vis-RS. In Figure 5f, the inflection point at 480 nm and the slope of the reflectance curve of the yellow layer fit with published reference spectra for orpiment is shown (Aceto et al., 2014; Cavaleri, Giovagnoli, & Nervo, 2013). Orpiment is found locally in Egypt associated with gold and silver ores (in Edfu and the Eastern Desert) or in copper ores (Saini mines), in hot-spring deposits, and volcanic sublimation, but others have reported that orpiment was imported from Syria or Asia Minor (Abdrabou et al., 2017; Bonizzoni et al., 2011; Bonizzoni et al., 2018; Bracci et al., 2015; Davies, 1995; Gard et al., 2020; Sakr, Ghaly, Abdulla, Edwards, & Elbashar, 2020; Scott et al., 2004; Scott, Warmlander, Mazurek, & Quirke, 2009). Historically, its earliest findings are dated to the 2nd Dynasty (Colinart, 2001) and several later findings in Egyptian artifacts have been reported (Abdrabou et al., 2017; Abdrabou, et al., 2022; Ambers, 2004; Amenta, 2014; Bonizzoni et al., 2011; Brunel-Duverger et al., 2019; Colinart, 2001) particularly during the 18th Dynasty, when it was extensively used to give a brilliant yellow, gold-like color with a shiny glaze, so it has been described as royal yellow (Sakr et al., 2020).

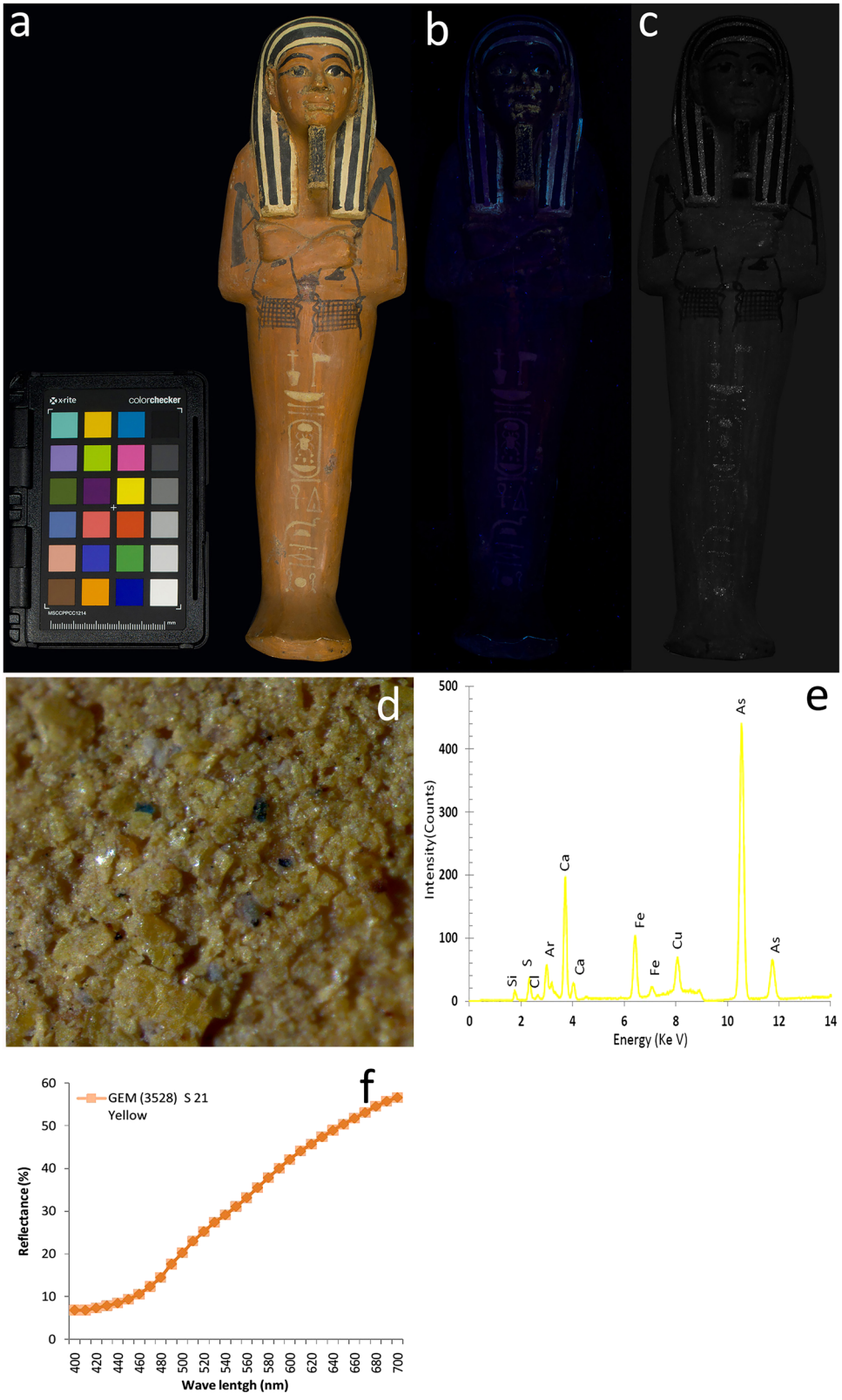

Figure 5: Analytical characterization of the yellow painted layer (Object GEM 3528, Spot 21): (a) visible image; (b) UV luminescence image; (c) VIL image; (d) an optical micrograph; (e) XRF spectrum; and (f) visible reflectance spectrum.

3.1.3 Red Painted Layers

All the red painted layers appeared darker in the UV-induced luminescence (UVL) images, which may suggest that the red pigment is red ochre, consistent with the strong quenching properties of the iron-based pigment (McCarthy, 2001). The microscopic examination showed the presence of some single particles of yellow pigment in some red paint areas (Figure 6a), which may be due to the use of dirty brushes or could be added to achieve a higher intensity of the red sensation. The results of XRF analysis for some points on the red painted layers (Figure 6b) showed the presence of Fe, Ca, As, Si, and S with a high intensity, in addition to a small amount of aluminum (Al). The presence of As and S is clearly related to the single grains of orpiment that are shown by the microscopic examination. The presence of Fe, Ca, Si, and Al provides strong evidence for the presence of red ochre, as confirmed by Vis-RS (Figure 5c), which displayed a sigmoid shape with an absorption band between 400 and 500 nm, a sharp positive slope between 550 and 600 nm, and an inflection point at 580 nm, which are indicative of red ochre (Abdrabou et al., 2022; Aceto et al., 2014; Cavaleri et al., 2013; Edreira et al., 2001; Guglielmi, Andreoli, Comite, Baroni, & Fermo, 2021; Miriello et al., 2018). Finally, applying XRD to the red painted layers showed that, apart from quartz, the presence of hematite is detected, in accordance with the attribution made by Vis-RS and XRF. The red areas are all colored with hematite (α Fe_2O_3), the main chromophore found in red ochres, and they contain a small proportion of other crystals, including quartz, and are better described as ochres rather than as pure hematite. This is in keeping with the other evidence from other Egyptian contexts, where red ochres are by far the most commonly reported red pigment. Red ochre was used to create a red color on wooden artifacts in ancient Egypt, according to many works (Bonizzoni et al., 2018; Lee & Quirke, 2000; Pagès-Camagna & Guichard, 2010).

3.1.4 White Painted Layers

The microscopic examination revealed the presence of some single particles of the blue and yellow pigments in the white painted layer (Figure 7a). The blue single particles appeared as bright white in the VIL image, which refers to the Egyptian blue pigment. The results of XRF analysis for some points on the white painted layers (Figure 7b) showed the presence of Ca and S with a high intensity, in addition to a small amount of Si, As, Fe, and Cu. The presence of Ca and S provides strong evidence for the presence of calcium-based pigments such as calcium sulfate. The presence of As and S is clearly related to the single grains of orpiment that are shown by the microscopic examination, while silicon and copper are detected in the white areas, clearly related to the single particles of Egyptian blue that are shown by VIL imaging. At some times, the ancient Egyptians added Egyptian blue to the white colors to achieve a higher intensity of the white sensation (Edreira, Feliu, Fernández-Lorenzo, & Martín, 2003). Finally, applying XRD to the white painted layers (Figure 7c) showed that, apart from quartz and weddellite (calcium oxalate), the presence of gypsum is detected, in accordance with the attribution made by XRF. Calcium-based pigments such as calcite, gypsum, and huntite were the most commonly used white pigments in Egyptian painting and have been reported in many works to create a white color on wooden artifacts (Ambers, 2004; Bonizzoni et al., 2011; Heywood, 2001).

3.1.5 Black Painted Layers

IR images strongly suggest the presence of carbon-based black in the black paint areas, as carbon is opaque under infrared emission and appears dark (Abdrabou et al., 2017). The microscopic investigation of the black pigment indicated the fineness and evenness of particles and did not show any fibrous structure, so it is possible to exclude the burnt vegetable origin of the black pigment (Abdrabou et al., 2018). In addition, some shawabtis (GEM 3503–3511) showed some single particles of orpiment pigments in the black painted layer, which may be due to the use of dirty brushes. In XRF analysis, phosphorus was detected in the black

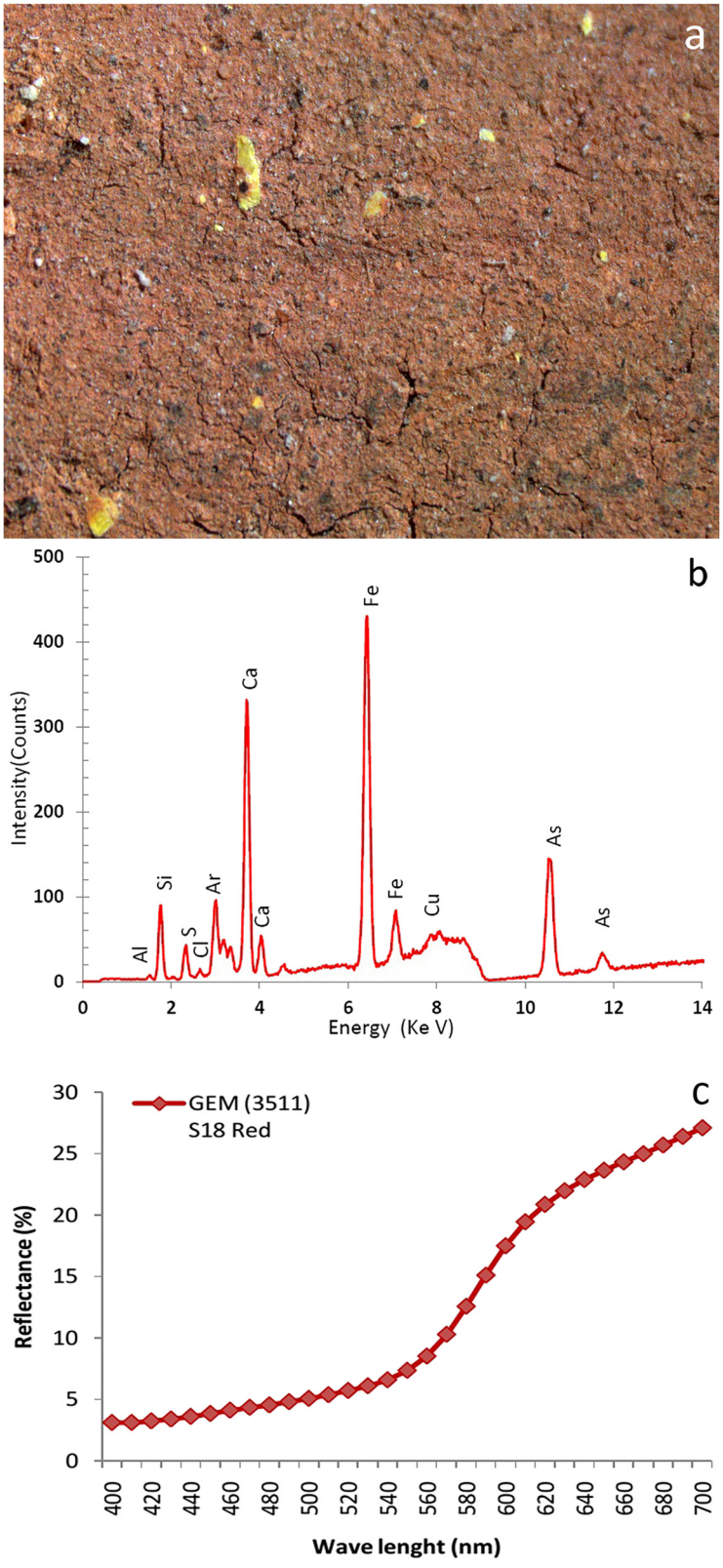

Figure 6: Characterization of the red painted layer (Object GEM 3511, Spot 18): (a) An optical micrograph; (b) XRF spectrum; and (c) visible reflectance spectrum.

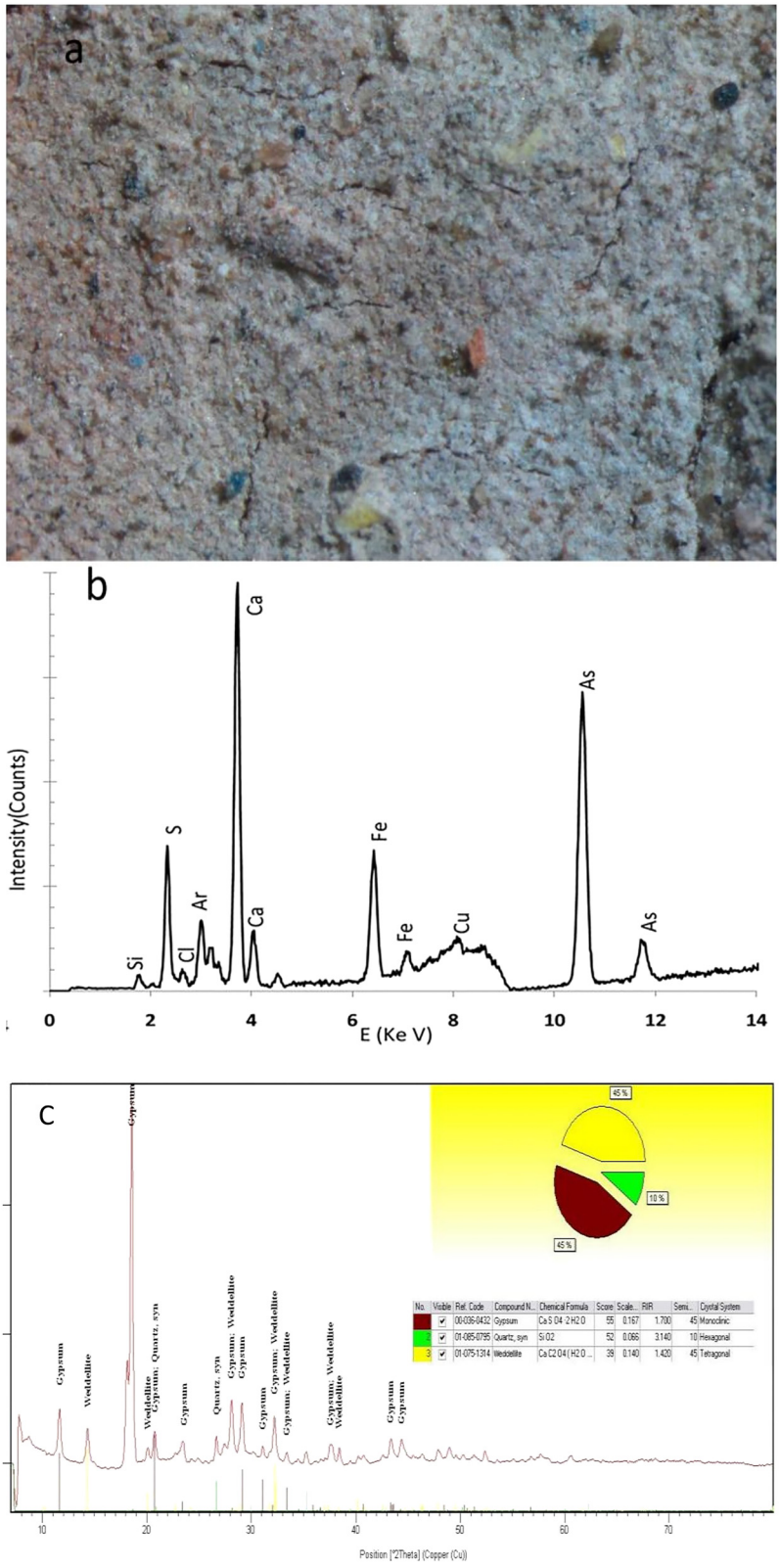

Figure 7: Characterization of the white painted layer (Object GEM 3503): (a) An optical micrograph; (b) XRF spectrum; and (c) XRD pattern.

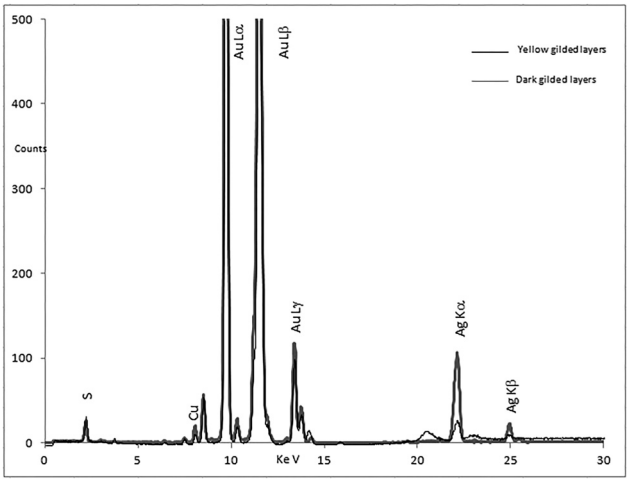

Figure 8: Comparing the obtained XRF spectra for yellow and dark areas of gilding.

painted layers of shawabtis GEM no. 3503 and 3511. This result provides evidence for the presence of carbon obtained from animal origins that is most likely bone black, which is one of the oldest pigments known to humans and was originally made by charring animal bones (Abdrabou et al., 2018; Mahmoud, 2014), while phosphorus was not detected in the XRF results from the black painted layers of the other shawabtis, making it most likely that they are of lamp black or soot, produced by the combustion of vegetable matter or oil (Ambers, 2004; Lee & Quirke, 2000).

3.1.6 Gilded Layers

The majority of the gold used in ancient Egypt was obtained from alluvial deposits and from quartz rock found between the Nile and the Red Sea (Colinart, 2001). Their composition ranged from very pure to those containing at least 40% of silver (electrum) and copper, with percentages not exceeding 1.5%. The majority of Tutankhamun's golden objects are gilded, either with gold foil or gold leaf applied over a firm support to achieve the rich appearance of solid gold (Abdallah, Abdrabou, & Kamal, 2018; Abdrabou et al., 2018; James, 1972). There are some gilded wooden shawabtis among them, with varying degrees of color ranging from bright yellow to reddish brown. According to the semiquantitative XRF results, the gilded layers with a bright yellow color have a similar composition and are composed of pure gold (Au) ranging from 99.2 to 98.5%, with less than 1% of Ag and Cu. The gilded layers with a reddish brown color exhibit a high Ag content that reaches 9%. The XRF spectra obtained for the yellow and dark colors were compared. XRF spectra (Figure 8) showed an increase in the Ag intensity in the dark areas of the gilded layers, with no significant change in the S and Cu intensities. The increase of Ag on the dark color of the gilded layers with the presence of S suggests the formation of distinct silver sulfide complexes, namely, AgAuS and Ag_3AuS_2, which correspond with previously published data for some dark gold Egyptian leafs/foils (Abdrabou, El Hadidi, Hamed, & Abdallah, 2018; Frantz & Schorsch, 1990; Hatchfield & Newman, 1991; Rifai & El Hadidi, 2010; Tissot, et al., 2015).

3.2 Analysis of Previous Restoration Materials

Table 4 shows a summary of the UVL imaging, XRF, and FTIR analysis results of the previous restoration material samples.

Table 4: : Summary for UVL imaging, XRF and FTIR analysis results of four samples from the previous restoration materials

Sample no	Object. no	UVL imaging	Elements detected by XRF	IR bands (cm^{-1})
1	GEM 3452JE 60807	Yellow	—	3,437, 2,970, 1,732, 1,653, 1,454, 1,278, 839
2		Green	—	3,427, 2,916, 1,695, 1,462, 1,379, 1,273, 1,173, 1,051, 728
3	GEM 3467JE 60813	Green	—	3,427, 2,916, 1,695, 1,462, 1,379, 1,273, 1,173, 1,051, 728
4	GEM 3651JE 60783	Very dark	**Fe, S, Zn, Ba, Ca**, Sr	2,916, 1,463, 1,124, 1,080, 904, 794, 728, 669, 609

Note: Elements in boldface are correlated to the main pigment mineral.

A UVL image (Figure 9b) revealed the presence of a yellowish emission from luminescent materials on the gilded surface (Object GEM 3452). This luminescence probably relates to cellulose nitrate (Grant, 2000) used in the previous restoration interventions made by Lucas during the discovery of the tomb, as Carter mentioned in his handwritten object cards. As shown in Figure 8c, the infrared spectrum of this material (sample 1) proved the presence of celluloid (bands at 3,437 cm^{-1} (O–H), 2,970 cm^{-1} (C–H), 1,732 cm^{-1} (C═O), 1,653 cm^{-1} (N–O), 1,454 cm^{-1} (C–H), 1,278 cm^{-1} (N–O), and 839 cm^{-1} (N–O) (Derrik et al., 1999) a resin used frequently as an adhesive, consolidant, and coating of artifacts in many applications for the first half of the 20th century. Due to its disadvantageous properties such as flammability and tendency to yellow, it is no longer used for the consolidation of artifacts (Unger, Schniewind, & Unger, 2001).

As shown in Figure 10b, UVL revealed the presence of a greenish emission from luminescent materials on the gilded surface (Object GEM 3467), and its presence is much more extensive than what was discernible with the naked eye (Figure 10a). This luminescence presumably relates to the use of rosin mixed with paraffin wax in the previous restoration interventions as mentioned in previous work (Abdrabou et al., 2018) The infrared spectrum of this material (sample 2 and 3) proved the presence of rosin (bands at 3,427, 1,695, 1,462, 1,379, 1,273, 1,173, and 1,051 cm^{-1}, Figure 10c) mixed with paraffin wax (bands at 2,926, 1,462, and 729 cm^{-1}, Figure 10c), (Abdrabou et al., 2019; Derrik et al., 1999). Rosin, a natural organic resin, has been used frequently as a surface treatment agent and in mixtures with waxes for filling cracks and voids in wood artifacts in recent decades (Abdallah, Kamal, & Abdrabou, 2016; Abdrabou et al., 2018; Unger et al., 2001). As for the previous yellow plaster fill material used in the object (GEM 3651), the UVL image makes these areas clearly visible as they do not emit any fluorescence under UV light and appear as characteristic black spots. The XRF spectrum revealed the presence of Fe, which may indicate the presence of modern iron-based pigments. Small amounts of S, Zn, and Ba are also observed. These elements suggest the use of lithopone ($ZnS + BaSO_4$), which was confirmed by XRD analysis. In the infrared spectrum of sample 4, yellow-based pigments (bands at 1,080, 904, and 794 cm^{-1}) were detected, bound by paraffin wax (bands at 2,916, 1,463, and 728 cm^{-1}). In the same spectrum, the presence of sulfate groups (SO_4) at 1,124, 669, and 609 cm^{-1} were also observed. These results indicate the use of different materials for these shawabtis during several restoration interventions from the discovery of the tomb in 1922 until their transportation to the GEM CC in 2016.

4 Conclusion

The use of an imaging-based protocol combined with data from single-spot techniques such as XRF and Vis-RS, as well as complementary results from XRD and FTIR, provided an excellent insight into the chemical compositions of the materials used for the pictorial polychrome layers of the studied shawabtis and presented a panoramic view of the previous restoration materials and their distribution on the shawabtis. In general, the findings can be used to explain the ancient technology of King Tutankhamun's polychrome wooden shawabtis.

The results revealed that the materials used for the original polychrome layers of the studied shawabtis were nearly identical to those used in ancient Egyptian polychrome artifacts with respect to a chromatic palette and the painting technique. The chromatic palette used in these shawabtis was identified as red ochre for the red painted layers, cuprorivaite mixed with gypsum for the blue painted layers, cuprorivaite mixed with calcite and quartz for greenish hue areas, orpiment for the yellow painted layer, and gypsum for the white painted layer. Carbon obtained from charred bone black and lamp black or soot was used for the black painted layers. The variation in the composition of gilded layers is in agreement with the composition of the other ancient Egyptian gold leaf previously determined. The application of imaging techniques provided useful information about the spatial distribution of pigments, in particular VIL, which allowed the spatial distribution of the surviving Egyptian blue pigment to be mapped. Moreover, UVL presented a panoramic view of the spatial distribution of the materials used in the previous restoration interventions, providing necessary data for future conservation work. This study provided preliminary information

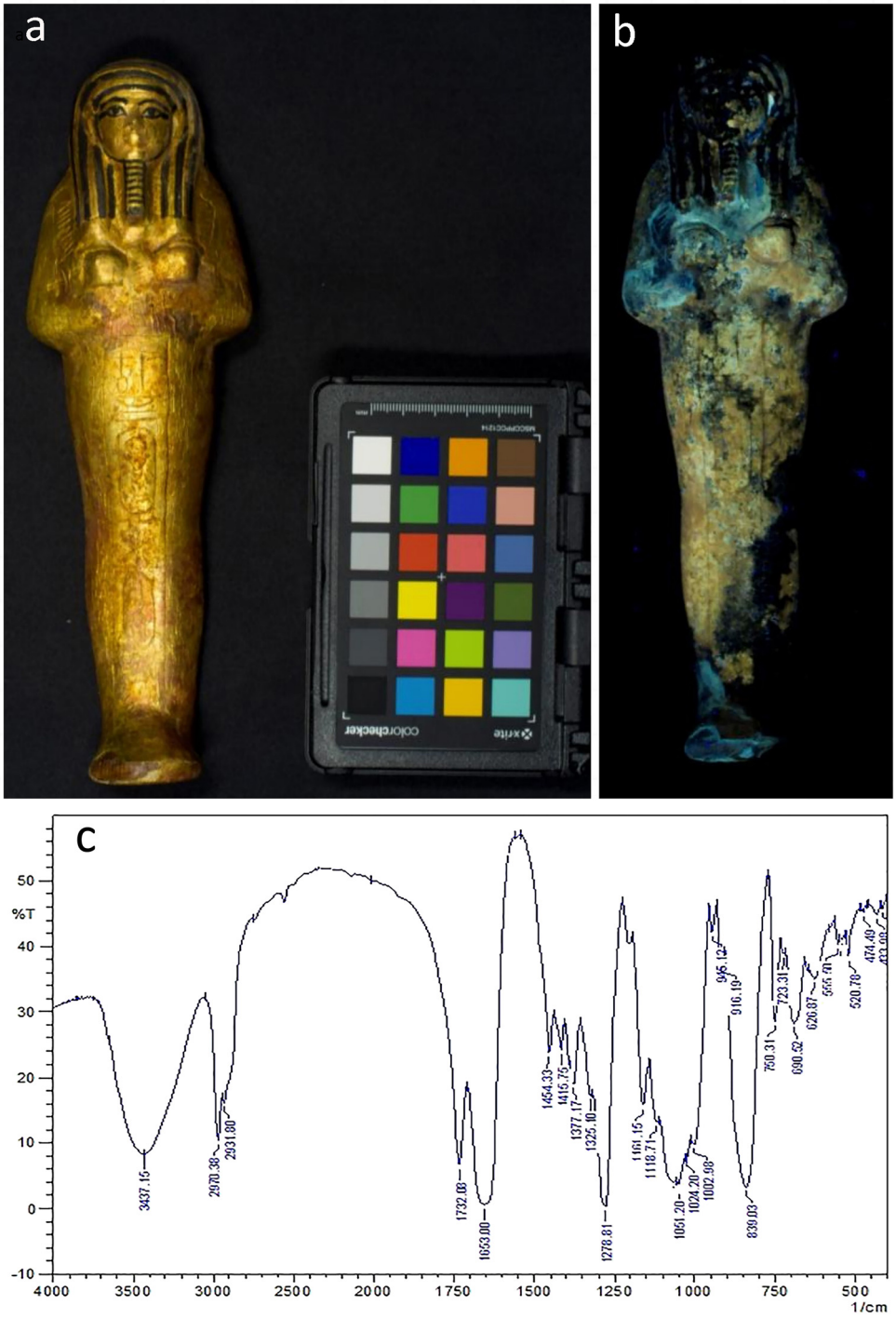

Figure 9: Analytical characterization of the previous consolidation material on the outer surface of Object GEM 3452: (a) visible image; (b) UV luminescence image; and (c) FTIR spectrum of sample 1.

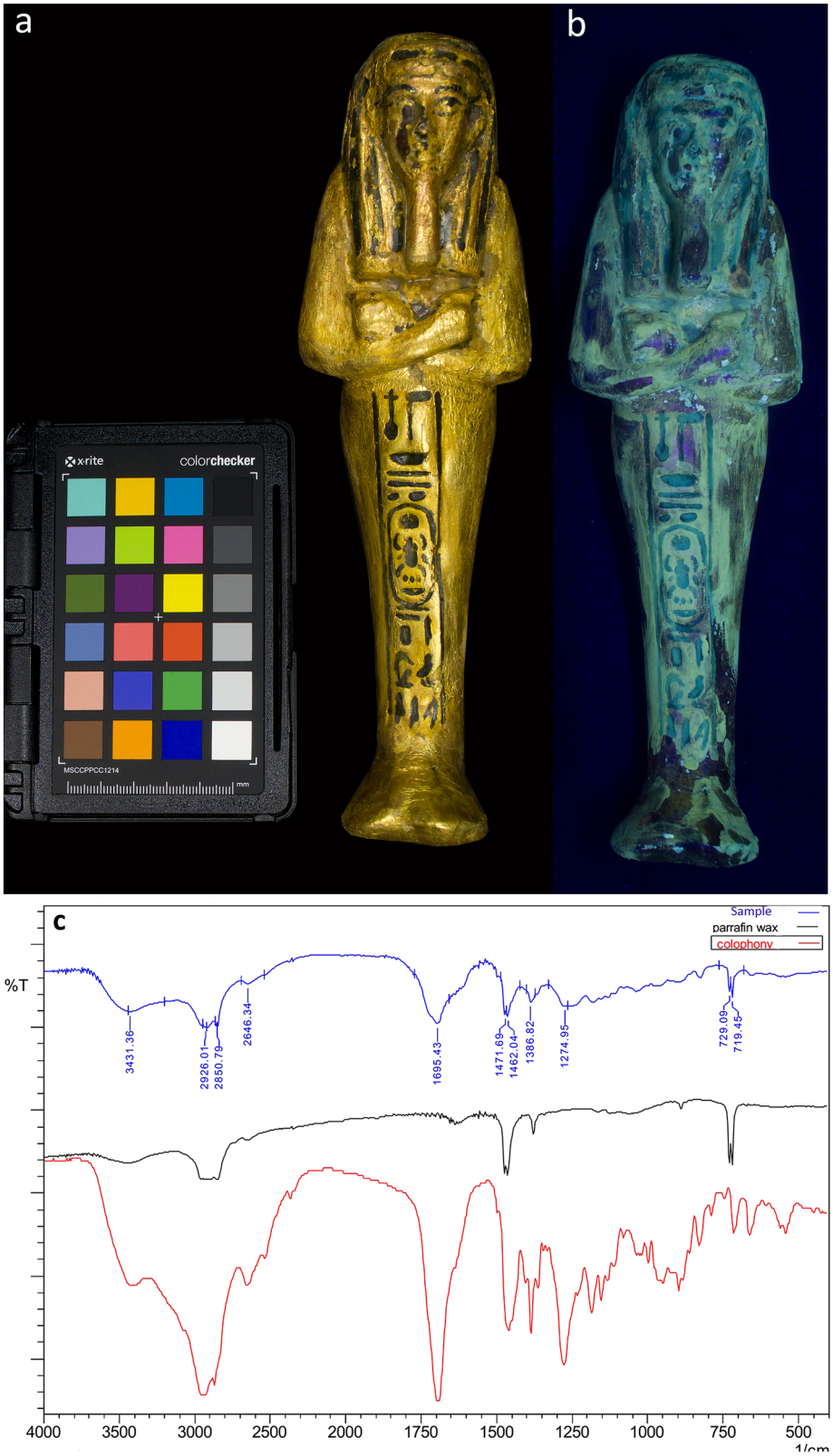

Figure 10: Analytical characterization of the previous resinous fills on the outer surface of Object GEM 3467: (a) visible image; (b) UV luminescence image; and (c) FTIR spectrum of sample 2.

concerning the original materials used in some polychrome wooden shawabtis of King Tutankhamun and the materials added during the previous treatment interventions, which provides not only important information for the study of polychrome wooden shawabtis from the same collection of Tutanhkamun and other periods in ancient Egypt but also essential data for the follow-up treatment and conservation works of these shawabtis.

Acknowledgments: The authors thank Mr Hassan Zidan (XRD Lab at GEM.CC) for his assistance. The authors thank Maj. General/Atef Moftah, General Supervisor of the Grand Egyptian Museum (GEM) and the surrounding area.

Funding information: Authors state no funding involved.

Author contributions: All authors have accepted responsibility for the entire content of this manuscript and approved its submission.

Conflict of interest: Authors state no conflict of interest.

Data availability statement: All data generated or analyzed during this study are included in this published article.

References

Abadir, M. I. (2014). *Experimental study of the Egyptian blue degradation by the copper chloride cancer, Bachelor Degree in chemical engineering*. Barcelona: Escola Tècnica Superior d'Enginyeria Industrial de Barcelona, Universitat politecnica de Catalunya (UPC).

Abdallah, M., & Abdrabou, A. (2018). Tutankhamen's small shrines (naoses): Technology of woodworKing and identification of wood species. *International Journal of Conservation Science*, *9*(1), 91–104.

Abdallah, M., Abdrabou, A., & Kamal, H. M. (2018). Analytical study and conservation processes of Tutankhamen decorated stick: A case study. *Scientific culture*, *4*(1), 93–100.

Abdallah, M., Abdrabou, A., & Kamal, H. M. (2020). Multiscientific analytical approach of polychrome greco-roman palette applied on a wooden model naos: Case study. *Mediterranean Archaeology and Archaeometry*, *20*(2), 45–65.

Abdallah, M., Kamal, H., & Abdrabou, A. (2016). Investigation, preservation and restoration processes of an ancient Egyptian wooden offering table. *International Journal of Conservation Science*, *7*(4), 1047–1064.

Abdrabou, A., Abdallah, M., & Kamal, H. M. (2017). Scientific investigation by technical photography, OM, ESEM, XRF, XRD and FTIR of an ancient Egyptian polychrome wooden coffin. *Conservar Património*, *26*, 51–63.

Abdrabou, A., Abdallah, M., Nabil, E., Matsuda, Y., & Kamal, H. M. (2019). Preliminary investigation of the materials and techniques used in a decorated wooden stick of King Tutankhamun. *Conservar Património*, *30*, 9–19.

Abdrabou, A., Abdallah, M., Shaheen, I. A., & Kamal, H. M. (2018). Investigation of an ancient Egyptian polychrome wooden statuette by imaging and spectroscopy. *International Journal of Conservation Science*, *9*(1), 39–54.

Abdrabou, A., El Hadidi, N. M., Hamed, S., & Abdallah, M. (2018). Multidisciplinary approach for the investigation and analysis of a gilded wooden bed of King Tutankhamun. *Journal of Archaeological Science: Reports*, *21*, 553–564.

Abdrabou, A., Hussein, A., Sultan, G. M., & Kamal, H. M. (2022). New insights into a polychrome Middle Kingdom palette applied to a wooden coffin: A multidisciplinary analytical approach. *Journal of Cultural Heritage*, *54*, 118–129.

Accorsi, G., Verri, G., Bolognes, M., Armaroli, N., Clementi, C., Miliani, C., & Romani, A. (2009). The exceptional near-infrared luminescence properties of cuprorivaite (Egyptian blue). *Chemical Communications*, *23*, 3392–3394.

Aceto, M., Agostino, A., Fenoglio, G., Idone, A., Gulmini, M., Picollo, M., … Delaney, J. K. (2014). Characterisation of colorants on illuminated manuscripts by portable fibre optic UV-visible-NIR reflectance spectrophotometry. *Analytical methods*.

Ambers, J. (2004). Raman analysis of pigments from the Egyptian Old Kingdom. *Journal of Raman Spectroscopy*, *35*, 768–773.

Amenta, A. (2014). The Vatican Coffin project. In E. Pischikova, J. Budka, & K. Griffen (Eds.), *Thebes in the first millennium* (pp. 483–499). Cambridge: Cambridge Scholars Publishing.

Bonizzoni, L., Bruni, S., Gargano, M., Guglielmi, V., Zaffino, C., Pezzotta, A., … Ludwig, N. (2018). Use of integrated non-invasive analyses for pigment characterization and indirect dating of old restorations on one Egyptian coffin of the XXI dynasty. *Microchemical Journal*, *138*, 122–131.

Bonizzoni, L., Bruni, S., Guglielmi, V., Milazzo, M., … Neri, O. (2011). Field and laboratory multi-technique analysis of pigments and organic painting media from an Egyptian coffin (26th dynasty). *Archaeometry*, *53*(6), 1212–1230.

Bracci, S., Caruso, O., Galeotti, M., Iannaccone, R., Magrini, D., Picchi, D., … Porcinai, S. (2015). Multidisciplinary approach for the study of an Egyptian coffin (late 22nd/early 25th dynasty): Combining imaging and spectroscopic techniques. *SpectrochimicActa Part A: Molecular and Biomolecular Spectroscopy*, *145*, 11–522.

Brunel-Duverger, L., Laval, E., Lemasson, Q., Brodie-Linder, N., & Pagès-Camagna, S. (2019). The contribution of non-invasive and non-destructive techniques to the understanding of the 21st Dynasty Egyptian Yellow Coffins complex stratigraphy: Case of study of E 20043 from the Louvre Museum. *The European Physical journal Plus*, *134*, 1–11.

Carter, H. (1933). *The tomb of Tut ankh amen* (Vol. III ed.). London: Cassell and Company, Ltd.

Cavaleri, T., Giovagnoli, A., & Nervo, M. (2013). Pigments and mixtures identification by visible reflectance spectroscopy, youth in conservation of cultural heritage, YOCOCU 2012. *Procedia Chemistry*, *8*, 45–54.

Colinart, S. (2001). Analysis of inorganic yellow colour in ancient Egyptian painting. In W. V. Davies (Ed.), *Colour and painting in ancient Egypt* (pp. 1–4). London: The British Museum Press.

Corcoran, L. H. (2016). The color blue as an "Animator" in ancient Egyptian art. In R. B. Goldman (Ed.), *Essays in global color history*, Interpreting the Ancient Spectrum (pp. 41–67). Piscataway, New Jersey: Gorgias Press.

Cosentino, A. (2015). Practical notes on ultraviolet technical photography for art examination. *Conservar Património*, *21*, 53–62.

Daniels, V., Stacey, R., & Middleton, A. (2004). The blackening of paint containing Egyptian blue. *Studies in Conservation*, *49*, 217–230.

Davies, W. (1995). Ancient Egyptian timber imports: An analysis of wooden coffins in the BritishMuseum. In W. Davies & L. Schofield (Eds.), *Egypt, the Aegean and the Levant: Interconnections in the second millennium BC* (pp. 146–156). London: British Museum Press.

Derrik, R. M., Stulik, D., & Landy, M. J. (1999). *Infrared spectroscopy in conservation science*. Los Angeles: The Getty Conservation Institute.

Dyer, J., & Sotiropoulou, S. (2017). A technical step forward in the integration of visible-induced luminescence imaging methods for the study of ancient polychromy. *Heritage Science*, *5*, 24.

Dyer, J., Verri, G., & Cupitt, J. (2013). *Multispectral imaging in reflectance and photo-induced luminescence modes: A user manual* (1st ed.). Available from: http://www.britishmuseum.org/pdf/charismamultispectral-imaging-manual-2013.pdf.

Edreira, C. M., Feliu, J. M., Fernández-Lorenzo, F. C., & Martín, J. (2003). Spectroscopic study of Egyptian blue mixed with other pigments. *Helvetica Chimica Acta*, *86*, 29–49.

Edreira, M., Feliu, M., Fernández-Lorenzo, C., & Martín, J. (2001). Roman wall paintings characterization from Cripta del Museo and Alcazaba in Mérida (Spain): Chromatic, energy dispersive X-ray flurescence spectroscopic, X-ray diffraction and Fourier transform infrared spectroscopic analysis. *Analytica Chimica Acta*, *434*, 331–345.

Frantz, H. J., & Schorsch, D. (1990). Egyptian red gold. *Archeomaterials*, *4*, 133–152.

Ganio, M., Salvant, J., Williams, J., Lee, L., Cossairt, O., & Walton, M. (2015). Investigating the use of Egyptian blue in Roman Egyptian portraits and panels from Tebtunis, Egypt'. *Applied Physics A*, *121*(3), 813–821.

Gard, F. S., Bozzano, P. B., Santos, D. M., Daizo, M. B., Halac, E. B., & Reinoso, M. (2020). A multi-analytical approach for the study of the pigments used to decorate an Egyptian cartonnage from ptolemaic period. *Microscopy and Microanalsis*, *26*, 1–2.

Giménez, J. (2015). Egyptian blue and/or atacamite in an ancient Egyptian coffin. *International Journal of Conservation Science*, *6*(4), 573–586.

Grant, M. S. (2000). 'The use of ultraviolet induced visible-fluorescence in the examination of museum objects, Part II'. *Conserve O Gram*, *1*(9), 1–3.

Green, L. (2001). Colour transformations in ancient Egyptian pigments. In W. Davies (Ed.), *In colour and painting in ancient Egypt* (pp. 43–48). London: British Museum Press.

Guglielmi, V., Andreoli, M., Comite, V., Baroni, A., & Fermo, P. (2021). The combined use of SEM-EDX, Raman, ATR-FTIR and visible reflectance techniques for the characterisation of Roman wall painting pigments from Monte d'Oro area (Rome): An insight into red, yellow and pink shades. Environmental Science and Pollution Research, 1–19.

Hatchfield, P., & Newman, R. (1991). Ancient Egyptian gilding methods. In D. Bigelow, E. Cornu, G. Landre, & C. V. Home (Eds.), *Gilded wood conservation and history* (pp. 291–299). Madison CT: Sound View Press.

Hatton, G., Shortland, A., & Tite, M. (2008). The production technology of egyptian blue and green frits from the second millennium BCE Egypt and Mesopotamia. *Journal of Archaeological Science, 35*, 1591–604.

Heywood, A. (2001). The use of huntite as a white pigment in ancient Egypt. In W. Davies (Ed.), *Colour and painting in ancient Egypt* (pp. 5–9). London: The British Museum Press.

Hoving, T. (1978). *Tutankhamun: The untold story*. New York: Simon and Schuster.

Ismail, Y., Abdrabou, A., & Abdallah, M. (2016). A non-destructive analytical study and the conservation processes of Pharaoh Tutankhamun´s painted boat model. *International Journal of Conservation Science*, *7*(1), 15–28.

Jaksch, H., Seipel, W., Weiner, K., & El Goresy, A. (1983). Egyptian blue – cuprorivaite a windowto ancient Egyptian technology. *Naturwissenschaften*, *70*(11), 525–535.

James, T. G. H. (1972). Gold technology in ancient Egypt, mastery of metal working methods. *Gold Bulletin*, *5*, 38–42

Lee, L. (1997). *Investigation into degraded pigments on the Coffin of Amenemope, EA 22941*. British Museum Conservation Research Group CA1997/20.

Lee, L., & Quirke, S. (2000). Painting materials. In P. Nicholson & I. Shaw (Eds.), *Ancient Egyptian materials and technologies* (pp. 104–121). Cambridge: Cambridge University Press.

Mahmoud, H. (2014). Investigations by Raman microscopy, ESEM and FTIR-ATR of wallpaintings from Qasr el-Ghuieta temple, Kharga Oasis, Egypt. *Heritage Science*, *2*, 18–29.

Martinez, K., & Cupitt, J. (2005). VIPS – a highly tuned image processing software architecture. *IEEE International Conference on Image Processing* (pp. 574–577).

McCarthy, B. (2001). Technical analysis of reds and yellows in the tomb of Suemniwet, Theban tomb 92. In W. V. Davies (Ed.), *Colour and painting in ancient Egypt* (pp. 17–21). London: The British Museum Press.

Miriello, D., Bloise, A., Crisci, G. M., De Luca, R., De Nigris, B., Martellone, A., … Ruggieri, N. (2018). Non-destructive multi-analytical approach to study the pigments of wall painting fragments reused in mortars from the archaeological site of Pompeii (Italy). *Minerals*, *8*(134), 1–15.

Mirti, P., Appolonia, L., Casoli, A., Ferarri, R., Laurenti, E., Amizano, A., & Chiari, G. (1995). Spectrochemical and structural studies on a roman sample of Egyptian Blue. *Spectrochimica Acta, Part A: Molecular and Biomolecular pectroscopy*, *51*(3), 437–46.

Pagès-Camagna, S., & Guichard, H. (2010). Egyptian colours and pigments in French collections: 30 years of physicochemical analyses on 30 objects. In J. Dawson, C. Rozeik, & M. Wright (Eds.), *Decorated surfaces on ancient Egyptian objects technology, deteriorationand conservation* (pp. 25–31). London: Archetype Publications.

Pradell, T., Salvado, N., Hatton, G., & Tite, M. (2006). Physical processes involved in production of the ancient pigment, Egyptian blue. *Journal of the American Ceramic Society, 89*(4), 1426–1431.

Reeves, N. (1990). *The complete Tutankhamen* (*the King-the Tomb-the Treasury*). Cairo: The American University in Cairo Press.

Riederer, J. (1977). Egyptian blue in artists. In E. FitzHugh (Ed.), *Pigments* (pp. 23–45). Oxford: Oxford University Press.

Rifai, M., & El Hadidi, N. M. (2010). Investigation and analysis of three gilded wood samples from the tomb of Tutankhamun. In J. Dawson, C. Rozeik, & M. M. Wright (Eds.), *Decorated surfaces on ancient Egyptian objects technology, deterioration and conservation* (pp. 16–24). London: Archetype Publications.

Sakr, A. A., Ghaly, M. F., Abdulla, M., Edwards, H., & Elbashar, Y. H. (2020). A new light on the grounds, pigments and bindings used in ancient Egyptian cartonnages from Tell Al Sawa, Eastern Delta, Egypt. *Jornal of Optics*, *49*(2), 230–247.

Schneider, H. (1977). *Shabtis: An Introduction to the history of ancient Egyptian funerary statuettes, with a catalogue of the collection of Shabtis in the National Museum of Antiquities at Leiden*. Leiden: Rijksmuseum van Oudheden.

Scott, D. A., Dodd, L. S., Furihata, J., Tanimoto, S., Keeney, J., Schilling, M. R., … Cowan, E. (2004). An ancient Egyptian Cartonnage Broad Collar: Technical examination of pigments and binding. *Studies in Conservation, 49*(3), 177–192.

Scott, D., Warmlander, S., Mazurek, J., & Quirke, S. (2009). Examination of some pigments, grounds and media from Egyptian cartonnage fragments in the Petrie Museum, University College London. *Journal of Archaeological Science, 36*(3), 923–932.

Stuart, B. H. (2007). *Analytical techniques in materials conservation*. England: Wiley.

The Griffith institute (2000–2004). *Tutankhamun: Anatomy of an excavation, the Howard carter archives, handwritten object cards by H. Carter*. [Online] Available at: http://www.griffith.ox.ac.uk/gri/carter/.

Tissot, I., Troalen, L., Manso, M., Ponting, M., Radtke, M., Reinholz, U., … Guerra, M. F. (2015). A multi-analytical approach to gold in Ancient Egypt: Studies on provenance and corrosion. *Spectrochimica Acta Part B, 108*, 75–82.

Unger, A., Schniewind, A., & Unger, W. (2001). *Conservation of wood artefacts, hand book*. Berlin Heidelberg: Springer-Verlag.